



# Reaction-rate distribution at large currents in porous electrodes

Zhiqiang Chen<sup>a,b</sup>, Dmitri L. Danilov<sup>a,b,\*\*</sup>, Rüdiger-A. Eichel<sup>b,c</sup>, Peter H.L. Notten<sup>a,b,d,\*</sup>

<sup>a</sup> Eindhoven University of Technology, Eindhoven, 5600, MB, the Netherlands

<sup>b</sup> Fundamental Electrochemistry (IEK-9), Forschungszentrum Jülich, Jülich, D-52425, Germany

<sup>c</sup> RWTH Aachen University, Aachen, D-52074, Germany

<sup>d</sup> University of Technology Sydney, Broadway, Sydney, NSW, 2007, Australia

## HIGHLIGHTS

- Analytical investigation on reaction-rate and current distributions in porous electrode.
- Three sets of solutions for different currents and electrode design parameters.
- Effective conductivities and currents shift reaction-rate and current distributions.

## ARTICLE INFO

### Keywords:

Reaction-rate distribution  
Current-density distribution  
Porous electrodes  
Li-ion batteries

## ABSTRACT

Reaction-rate distribution inside porous electrodes influences the overall performance of Li-ion batteries. The design parameters greatly determine the reaction-rate distribution. Therefore, investigating the relationship between the design parameters and the reaction-rate distribution is vital for improving battery performance. In the present paper, the reaction-rate and current-density distributions are analytically derived across porous electrodes at a short time scale with a Tafel approximation of the Butler-Volmer equation. Three sets of solutions are obtained based on applied currents and design parameters of porous electrodes. In all three sets of solutions, the effective ionic and electronic conductivities are found to shift the reaction from the current-collector to the separator interface. The applied current also influences the reaction-rate and current-density distribution. High C-rates increase the nonuniformity of reaction-rate distribution and the non-linearity of the current distribution. In contrast, low C-rates benefit the uniformity of reaction and linearity of current density.

## 1. Introduction

Li-ion batteries (LIBs) nowadays have become ubiquitous in our daily life. Their applications range from mobile electronics to electric vehicles and stationary energy storage [1,2]. As an energy storage device, the energy and power are expected to be as high as possible to meet the rapidly increasing demands. The manufacturers widely adopt the porous electrode structure to increase the energy/power density due to the numerous advantages [3,4], such as the enlarged interfacial areas, reduced ionic diffusion pathways, increased heat dissipation rate, etc. However, the multiple physical and (electro)chemical processes inside porous electrodes make optimizing the battery design and performance challenging. An in-depth understanding of porous electrodes is therefore highly needed.

One of the most complicated properties is the reaction-rate distribution inside the porous electrode [5–9]. At a short-time scale, the reaction-rate distribution can be derived analytically by a porous electrode model. Linear or Tafel approximation of the Butler-Volmer equation has been applied to help the equation derivations at the low or high overpotential [6,7]. It was proposed that the reaction-rate distribution across porous electrodes is determined by four dimensionless ratios [5–7], namely the dimensionless current density, the dimensionless exchange current, the ratio of the charge transfer coefficient, and the ratio of effective conductivities. To perform a more detailed investigation, Chen et al. [8] applied a linear approximation to the Butler-Volmer equation. An explicit analytical solution was derived for the reaction-rate and current distributions inside the porous electrode. The effective ionic and electronic conductivities are critical in shaping the

\* Corresponding author. Eindhoven University of Technology, Eindhoven, 5600, MB, the Netherlands.

\*\* Corresponding author. Eindhoven University of Technology, Eindhoven, 5600, MB, the Netherlands.

E-mail addresses: [d.danilov@tue.nl](mailto:d.danilov@tue.nl) (D.L. Danilov), [p.h.l.notten@tue.nl](mailto:p.h.l.notten@tue.nl) (P.H.L. Notten).

<https://doi.org/10.1016/j.jpowsour.2023.233495>

Received 1 April 2023; Received in revised form 21 July 2023; Accepted 5 August 2023

Available online 19 August 2023

0378-7753/© 2023 The Authors. Published by Elsevier B.V. This is an open access article under the CC BY license (<http://creativecommons.org/licenses/by/4.0/>).

reaction-rate and current distributions. It was found that the effective ionic/electronic conductivity also has a saturated effect on shaping the reaction-rate and current distributions, suggesting that improving the battery performance by increasing conductivities should take the limit into consideration. At high overpotential, the linear approximation are not applicable anymore. In contrast, the Tafel approximation should be considered. However, the details of the reaction-rate and current distributions when Tafel approximation is applied are not yet covered by literature.

The present paper applies a Tafel approximation to the Butler-Volmer equation to derive the reaction-rate and current distributions across the porous electrode analytically. Three sets of solutions are obtained. The electrode parameters and applied current are found to determine the selection of a particular solution. These analytical solutions ultimately help to investigate the reaction-rate and current distributions inside porous electrodes.

## 2. Model development

The present paper considers a battery cell with a single porous electrode. Fig. 1 shows a layout of the cell, which includes a metallic Li foil, a porous separator, and a porous graphite-based electrode immersed in a liquid electrolyte. For simplification, the graphite will be represented by C. The larger gray and smaller black circles denote the electrode active particles and the conducting additives, respectively.  $\delta$  and  $L$  represent the thickness of the separator and the whole cell. The thickness of the C-based porous electrode, therefore, equals to  $L - \delta$ . The Li-metal/separator interface, the separator/C-based porous-electrode interface and the C-based-electrode/current collector interface are defined as LS, SC, and CC interfaces at  $x = 0$ ,  $x = \delta$ , and  $x = L$ , respectively.

At the moment when the current begins to be applied, the cell is assumed to be in a pseudo-equilibrium state. Therefore, all derivatives related to Li concentration gradients in both the electrode and electrolyte can be ignored. The system of equations can then be expressed as

$$i_1 = -\sigma_c \frac{d\Phi_1}{dx}, i_1(\delta) = 0, i_1(L) = I, \quad (1)$$

$$i_2 = -\kappa_c \frac{d\Phi_2}{dx}, i_2(\delta) = I, i_2(L) = 0, \quad (2)$$

$$\frac{di_2}{dx} = aFj_c = aI_c^0 \left[ \exp\left(\frac{\alpha F\eta^{ct}}{RT}\right) - \exp\left(-\frac{(1-\alpha)F\eta^{ct}}{RT}\right) \right], \quad (3)$$

$$\eta^{ct} = \Phi_1 - \Phi_2 - U_c(c_1^s), \quad (4)$$

$$i_1 + i_2 = I. \quad (5)$$

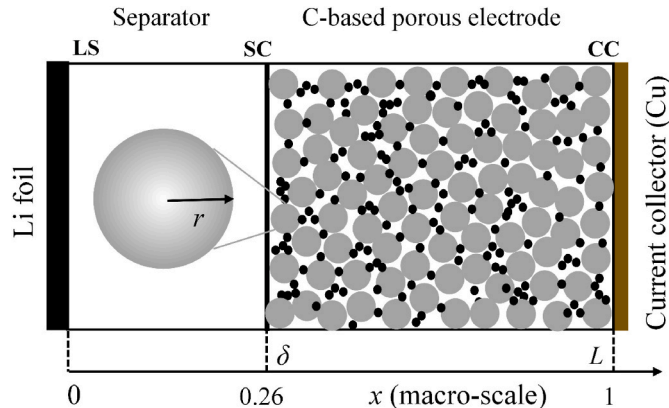


Fig. 1. Schematic representation of a C-based porous electrode/Li cell.

where  $i_1$  and  $i_2$  represent the electronic current and ionic current density ( $A \cdot m^{-2}$ ),  $\Phi_1$  and  $\Phi_2$  are electrical potentials (V) in the solid and liquid phases. Note that subscripts 1 and 2 denote properties in the solid and liquid phases.  $\sigma_c$  and  $\kappa_c$  are the effective electronic and ionic conductivity ( $S \cdot m^{-1}$ ) in the solid and liquid phases, respectively. The effective conductivity represents the actual moving pathway of species in a porous medium. Detailed explanations can be found elsewhere [10,11].  $\eta^{ct}$  stands for the charge-transfer overpotential (V) at the surface of active materials, and  $U_c$  is the equilibrium potential of the electrode active material (V).  $a$  is the specific area ( $m^2 \cdot m^{-3}$ ) in the porous electrode,  $j_c$  the reaction rate ( $mol \cdot m^{-2} \cdot s^{-1}$ ) for the charger-transfer reaction, and  $i_c^0$  is the exchange current density ( $A \cdot m^{-2}$ ).  $I$  is the applied current density ( $A \cdot m^{-2}$ ) to the cell, and  $R$  and  $T$  the universal gas constant ( $J \cdot mol^{-1} \cdot K^{-1}$ ) and absolute temperature (K), respectively.

Assuming that the overpotential is large enough, one exponent term in the Butler-Volmer equation vanishes (Tafel approximation). Considering a large positive overpotential, the second term (cathodic term) is, therefore, negligible.

$$j_c = \frac{i_c^0}{F} \left[ \exp\left(\frac{\alpha F\eta^{ct}}{RT}\right) - \exp\left(-\frac{(1-\alpha)F\eta^{ct}}{RT}\right) \right] \approx \frac{i_c^0}{F} \exp\left(\frac{\alpha F\eta^{ct}}{RT}\right). \quad (6)$$

Substituting Eq. (6) into Eq. (3) gives

$$\frac{di_2}{dx} = aFj_c = aI_c^0 \exp\left(\frac{\alpha F\eta^{ct}}{RT}\right). \quad (7)$$

Differentiating Eq. (7) once more and substituting derivatives of  $\Phi_1$  and  $\Phi_2$  (Eqs. (1) and (2)) give

$$\begin{aligned} \frac{d^2 i_2}{dx^2} &= aI_c^0 \frac{d \exp\left(\frac{\alpha F\eta^{ct}}{RT}\right)}{dx} = \frac{aI_c^0 \alpha F}{RT} \exp\left(\frac{\alpha F\eta^{ct}}{RT}\right) \frac{d\eta^{ct}}{dx} = \frac{\alpha F}{RT} \cdot \frac{di_2}{dx} \cdot \left( \frac{d\Phi_1}{dx} - \frac{d\Phi_2}{dx} \right) \\ &= \frac{\alpha F}{RT} \cdot \frac{di_2}{dx} \cdot \left( -\frac{i_1}{\sigma_c} + \frac{i_2}{\kappa_c} \right). \end{aligned} \quad (8)$$

Note that the derivative of  $U_c(c_1^s)$  vanishes because the  $Li^+$  concentration in the solid is constant for a short time interval. Using the current conservation in Eq. (5), Eq. (8) can then be rewritten as

$$\frac{d^2 i_2}{dx^2} = \frac{\alpha F}{RT} \cdot \frac{di_2}{dx} \cdot \left( \frac{i_2}{\kappa_c} - \frac{I - i_2}{\sigma_c} \right), i_2(\delta) = I, i_2(L) = 0. \quad (9)$$

Define

$$\begin{aligned} \gamma &= \frac{1/\sigma_c}{1/\sigma_c + 1/\kappa_c}, h^2 = \frac{\alpha F}{RT} \\ &\cdot \left( \frac{1}{\kappa_c} + \frac{1}{\sigma_c} \right), \text{ and normalized current } i_2'(x) = \frac{i_2(x) - I\gamma}{I} \end{aligned} \quad (10)$$

Eq. (9) can then be reformulated as

$$\frac{d^2 i_2'}{dx^2} = Ih^2 \cdot \frac{di_2'}{dx}, i_2'(\delta) = 1 - \gamma, i_2'(L) = -\gamma. \quad (11)$$

To reduce the order of Eq. (11), the following technique is used

$$p(i_2') = \frac{di_2'}{dx}, \frac{d^2 i_2'}{dx^2} = \frac{dp(i_2')}{dx} = \frac{dp(i_2')}{di_2'} \cdot \frac{di_2'}{dx}. \quad (12)$$

Substituting expression in Eq. (12) into the left-hand side of Eq. (11) gives

$$\frac{dp(i_2')}{di_2'} \cdot \frac{di_2'}{dx} = Ih^2 \cdot \frac{di_2'}{dx} \quad (13)$$

Simplifying Eq. (13) according to definition Eq. (12) leads to

$$\frac{dp(i_2')}{di_2'} = Ih^2 i_2'. \quad (14)$$

Integrating Eq. (14) gives the following expression

$$p(i_2(x)) - p(i_2(\delta)) = \frac{Ih^2}{2} [(i_2(x))^2 - (i_2(\delta))^2]. \quad (15)$$

Back-substitution of the definition from Eq. (12) into Eq. (15) yields

$$\frac{di_2(x)}{dx} - \frac{di_2(\delta)}{dx} = \frac{Ih^2}{2} [(i_2(x))^2 - (i_2(\delta))^2]. \quad (16)$$

Eq. (16) can be further simplified to

$$\begin{aligned} \frac{di_2(x)}{dx} &= \frac{Ih^2}{2} [(i_2(x))^2 - (i_2(\delta))^2] + \frac{di_2(\delta)}{dx} = \frac{Ih^2}{2} \left[ (i_2(x))^2 + \frac{2}{I^2 h^2} \frac{di_2(\delta)}{dx} \right. \\ &\quad \left. - (1-\gamma)^2 \right] = \frac{Ih^2}{2} \left[ (i_2(x))^2 + \frac{2}{I^2 h^2} \left( \frac{di_2(\delta)}{dx} - \frac{I^2 h^2}{2} (1-\gamma)^2 \right) \right]. \end{aligned} \quad (17)$$

According to Eq. (3), the following equation holds:  $\frac{di_2(\delta)}{dx} = aFj_c(\delta)$ . Note that  $j_c(\delta)$  represents the reaction rate at the SC interface. Substitution of this equation into Eq. (17) yields

$$\frac{di_2(x)}{dx} = \frac{Ih^2}{2} \left[ (i_2(x))^2 + \frac{2aF}{I^2 h^2} \left( j_c(\delta) - \frac{I^2 h^2}{2aF} (1-\gamma)^2 \right) \right]. \quad (18)$$

Defining  $\psi = j_c(\delta) - \frac{I^2 h^2}{2aF} (1-\gamma)^2$  and  $A^2 = \left| \frac{2aF}{I^2 h^2} \psi \right|$ , Eq. (18) can then be rewritten as

$$\frac{di_2(x)}{dx} = \frac{Ih^2}{2} [(i_2(x))^2 + sA^2]. \quad (19)$$

where  $s$  is a sign indicator based on the value of  $\psi$ . Parameter  $\psi$  determines the different branches of Eq. (19) and is named the Case-determining Condition (CDC). Three cases can therefore be distinguished according to the CDC. In case (i)  $\psi > 0$ , that is  $j_c(\delta) > \frac{I^2 h^2}{2aF} (1-\gamma)^2$ ,  $s$  is +1 and  $A^2 = \frac{2aF}{I^2 h^2} \psi$ . In case (ii),  $\psi < 0$ , that is  $j_c(\delta) < \frac{I^2 h^2}{2aF} (1-\gamma)^2$ , then  $s = -1$  and  $A^2 = -\frac{2aF}{I^2 h^2} \psi$ . In case (iii)  $A = 0$ . According to these three cases, the solutions of Eq. (19) vary.

### 2.1. Case (i)

Considering the first case, Eq. (19) can be rearranged as

$$\frac{di_2(x)}{(i_2(x))^2 + A^2} = \frac{Ih^2}{2} dx. \quad (20)$$

The solution of Eq. (20) has the following form

$$\frac{\left[ \operatorname{atan}\left(\frac{i_2(x)}{A}\right) - \operatorname{atan}\left(\frac{1-\gamma}{A}\right) \right]}{A} = \frac{Ih^2}{2} (x - \delta). \quad (21)$$

Resolving  $i_2(x)$  gives

$$i_2(x) = A \tan \left[ \frac{Ih^2}{2} A(x - \delta) + \operatorname{atan}\left(\frac{1-\gamma}{A}\right) \right]. \quad (22)$$

Eq. (22) agrees with the first boundary condition in Eq. (11). Introducing the second boundary condition gives

$$\tan \left[ \frac{Ih^2}{2} A(L - \delta) + \operatorname{atan}\left(\frac{1-\gamma}{A}\right) \right] = -\frac{\gamma}{A}. \quad (23)$$

Rearranging Eq. (23) yields

$$\frac{Ih^2}{2} A(L - \delta) + \operatorname{atan}\left(\frac{1-\gamma}{A}\right) + \operatorname{atan}\left(\frac{\gamma}{A}\right) = 0, \quad (24)$$

This equation may have a solution depending on parameter values. Now, differentiating Eq. (21) with respect to  $x$  results in

$$\frac{1}{1 + (i_2(x)/A)^2} \frac{di_2(x)}{dx} \frac{1}{A^2} = \frac{Ih^2}{2}. \quad (25)$$

From Eq. (25), the reaction rate can be expressed as

$$j_c(x) = \frac{1}{Fa} \frac{di_2}{dx} = \frac{I}{Fa} \frac{di_2}{dx} = \frac{I^2 h^2 A^2}{2Fa} \left[ 1 + \left( \tan \left[ \frac{Ih^2}{2} A(x - \delta) + \operatorname{atan}\left(\frac{1-\gamma}{A}\right) \right] \right)^2 \right]. \quad (26)$$

Replacing  $i_2(x)$  in Eq. (22) with  $i_2$  finally leads to

$$i_2(x) = i_2(x)I + I\gamma = AI \tan \left[ \frac{Ih^2}{2} A(x - \delta) + \operatorname{atan}\left(\frac{1-\gamma}{A}\right) \right] + I\gamma. \quad (27)$$

### 2.2. Case (ii)

Considering the second case, Eq. (19) can be rewritten as

$$\frac{di_2(x)}{(i_2(x))^2 - A^2} = \frac{Ih^2}{2} dx. \quad (28)$$

with an apparent solution

$$\frac{\left[ -\operatorname{atanh}\left(\frac{i_2(x)}{A}\right) + \operatorname{atanh}\left(\frac{1-\gamma}{A}\right) \right]}{A} = \frac{Ih^2}{2} (x - \delta), \quad (29)$$

where  $\tanh(y) = \frac{\exp(y) - \exp(-y)}{\exp(y) + \exp(-y)}$ . Expressing  $i_2(x)$  gives

$$i_2(x) = A \tanh \left[ -\frac{Ih^2}{2} A(x - \delta) + \operatorname{atanh}\left(\frac{1-\gamma}{A}\right) \right]. \quad (30)$$

which agrees with the first boundary condition in Eq. (11). Applying the second boundary condition produces

$$\tanh \left[ -\frac{Ih^2}{2} A(L - \delta) + \operatorname{atanh}\left(\frac{1-\gamma}{A}\right) \right] = -\frac{\gamma}{A}, \quad (31)$$

Rearranging Eq. (31) gives

$$-\frac{Ih^2}{2} A(L - \delta) + \operatorname{atanh}\left(\frac{1-\gamma}{A}\right) + \operatorname{atanh}\left(\frac{\gamma}{A}\right) = 0, \quad (32)$$

Eq. (32) may have a solution depending on parameter values. Then, differentiating Eq. (29) with respect to  $x$  obtains

$$-\frac{1}{1 - (i_2(x)/A)^2} \frac{di_2(x)}{dx} \frac{1}{A^2} = \frac{Ih^2}{2}. \quad (33)$$

from which the reaction rate is found as

$$j_c(x) = \frac{1}{Fa} \frac{di_2}{dx} = \frac{I}{Fa} \frac{di_2}{dx} = \frac{I^2 h^2 A^2}{2Fa} \left[ 1 - \left( \tanh \left[ -\frac{Ih^2}{2} A(x - \delta) + \operatorname{atanh}\left(\frac{1-\gamma}{A}\right) \right] \right)^2 \right]. \quad (34)$$

Replacing  $i_2(x)$  in Eq. (30) with  $i_2$  leads to

$$i_2(x) = i_2(x)I + I\gamma = AI \tanh \left[ \frac{Ih^2}{2} A(x - \delta) + \operatorname{atanh}\left(\frac{1-\gamma}{A}\right) \right] + I\gamma. \quad (35)$$

### 2.3. Case (iii)

Case  $A = 0$  gives

$$\frac{di_2(x)}{(i_2(x))^2} = \frac{Ih^2}{2} dx. \quad (36)$$

Thus

$$\frac{1}{i_2(x)} - \frac{1}{1-\gamma} = -\frac{Ih^2}{2} (x - \delta), \quad (37)$$

and

$$i_2(x) = \frac{1-\gamma}{1 + \frac{h^2(1-\gamma)}{2}(x-\delta)}. \quad (38)$$

Then differentiation of Eq. (38) gives

$$\frac{1}{(i_2(x))^2} \frac{di_2(x)}{dx} = \frac{h^2}{2}, \quad (39)$$

from which the reaction rate is expressed as

$$j_c = \frac{1}{Fa} \frac{di_2}{dx} = \frac{I}{Fa} \frac{di_2}{dx} = \frac{I^2 h^2}{2Fa} \left( \frac{1-\gamma}{1 + \frac{h^2(1-\gamma)}{2}(x-\delta)} \right)^2. \quad (40)$$

Replacing  $i_2(x)$  in Eq. (38) with  $i_2$  leads to

$$i_2(x) = i_2(x)I + I\gamma = \frac{(1-\gamma)I}{1 + \frac{h^2(1-\gamma)}{2}(x-\delta)} + I\gamma. \quad (41)$$

### 3. Experimental

The electrodes used in this paper were obtained from commercial 18650-type cylindrical batteries manufactured by Tianjin Lishen Battery Co., Ltd. These batteries were dismantled in an argon-filled glove box. Then pieces of the electrodes were taken out for the subsequent physical and electrochemical measurements. For the physical measurements, the thickness of electrodes and particle size were measured by a micrometer caliper and a scanning electron microscope. The thickness of a separator was also measured. For the electrochemical measurements, the graphite-based anode was selected and cut into discs with a diameter of 14 mm. 2032-type coin cells were subsequently assembled using the as-prepared graphite-based electrodes as working electrodes and Li metal foil as counter electrodes. A 2400-type Celgard separator (25  $\mu\text{m}$  thick) and 1 M LiPF<sub>6</sub> electrolyte in a solvent mixture of EC:DMC:DEC with a 1:1:1 volume ratio were used.

### 4. Results and discussion

As derived in Section 2, the current and reaction-rate distributions can be expressed by one of the three cases according to the adopted parameters. To find the exact case for a particular set of parameters, the value of CDC  $\psi$  has to be checked. Note that  $\psi = j_c(\delta) - \frac{I^2 h^2}{2aF}(1-\gamma)^2$ . However, it is challenging to obtain the value of  $\psi$  since the reaction rate at the separator/porous electrode interface  $j_c(\delta)$  is not explicitly expressed and influenced by multiple factors [8]. A simple situation is considered to help in illustration. As described in the reference [8], a large enough value of  $\sigma_c$  and  $\kappa_c$  will force the reaction rate to be evenly distributed across the porous electrode with a linear approximation of the Butler-Volmer equation. Here assuming a large and equal value of  $\sigma_c$  and  $\kappa_c$ , i.e.  $\sigma_c = \kappa_c$ , also leads to a uniform reaction-rate distribution for

the Tafel approximation. This assumption will be proven at the end of this section. In this situation, uniform reaction-rate distribution can be explicitly expressed as

$$j_c^u = -\frac{I}{a(L-\delta)F}. \quad (42)$$

With the situation ( $j_c(\delta) = j_c^u$ ), CDC  $\psi$  can be denoted as  $\psi^*$ , which is expressed as

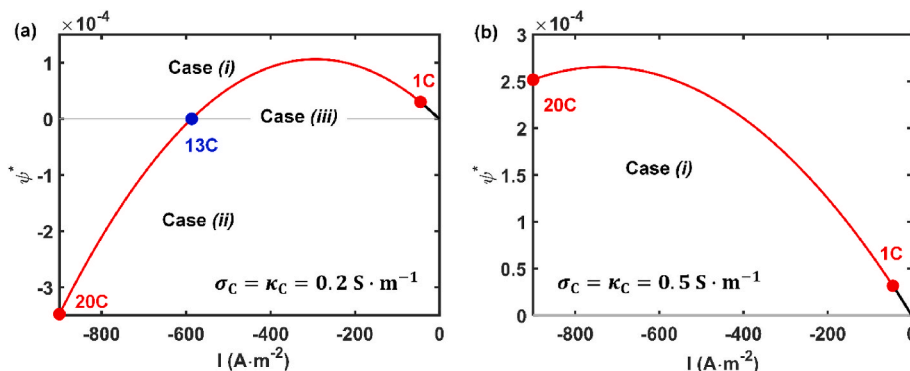
$$\psi^* = -\frac{I}{a(L-\delta)F} - \frac{I^2 h^2}{2aF}(1-\gamma)^2 = -\frac{I}{a(L-\delta)F} - \frac{\alpha(1/\sigma_c + 1/\kappa_c)I^2}{8aRT}. \quad (43)$$

Fig. 2 shows the specific CDC  $\psi^*$  in Eq. (43) as a function of the applied current density ( $I$ ) given values for (a)  $\sigma_c = \kappa_c = 0.2 \text{ S}\cdot\text{m}^{-1}$  and (b)  $\sigma_c = \kappa_c = 0.5 \text{ S}\cdot\text{m}^{-1}$ . The remaining parameter values are shown in Table 1. This specific CDC  $\psi^*$  is a quadratic function of the applied current  $I$ . Other parameters, such as  $a$ ,  $L-\delta$ ,  $\sigma_c$  and  $\kappa_c$  also influence the shape of the function curve. All three cases of CDC can occur, depending on the given parameter values. In Fig. 2a values of  $\sigma_c$  and  $\kappa_c$  are moderate. Then for current densities up to 13C ( $1\text{C} = 45 \text{ A}\cdot\text{m}^{-2}$ ), case (i) holds. For even larger currents (densities), case (ii) tends to occur. At 13C, case (iii) applies. In Fig. 2b where  $\sigma_c$  and  $\kappa_c$  are large, case (i) holds in most of the scenarios. For a completely general situation,  $j_c(\delta)$  is influenced by the battery parameters set and cannot be explicitly expressed. However, the dependence of the CDC on current (density),  $\sigma_c$  and  $\kappa_c$  should be similar. In most scenarios, case (i) shows the dominant role. Other factors, such as the specific area  $a$  and thickness of the porous electrode  $L-\delta$ , also play an important role, according to Eq. (43). Except the factors mentioned here, any other factors causing nonuniform reaction rate distribution also take part in the determination of the CDC, such as electrolyte concentration, Bruggeman coefficient, porosity, etc.

Fig. 3 shows the dependence of the reaction-rate  $j_c$  and current-density  $i_2$  distributions on the effective electronic and ionic conductivities ( $\sigma_c$  and  $\kappa_c$ ) when the applied current is 1C. In Fig. 3a–b,  $\kappa_c$  is kept as a constant  $10^{-2} \text{ S}\cdot\text{m}^{-1}$ , while  $\sigma_c$  changes from  $10^{-3}$  to  $10^{-1} \text{ S}\cdot\text{m}^{-1}$ . When

**Table 1**  
Parameter values used in the simulations.

Parameters	Values	Units
$a$	$2.05 \times 10^5$	$\text{m}^{-1}$
$i_c^0$	0.63	$\text{A}\cdot\text{m}^{-2}$
$R$	8.314	$\text{J}\cdot\text{mol}^{-1}\cdot\text{K}^{-1}$
$T$	298	K
$F$	96500	$\text{C}\cdot\text{mol}^{-1}$
$\delta$	$25 \times 10^{-6}$	m
$L$	$95 \times 10^{-6}$	m
$I$	$-450 \sim -22.5$	$\text{A}\cdot\text{m}^{-2}$
$\sigma_c$	$10^{-3} \sim 10^{-1}$	$\text{S}\cdot\text{m}^{-1}$
$\kappa_c$	$10^{-3} \sim 10^{-1}$	$\text{S}\cdot\text{m}^{-1}$



**Fig. 2.** The illustration of specific CDC  $\psi^*$  as a function of  $I$  at the condition of (a)  $\sigma_c = \kappa_c = 0.2 \text{ S}\cdot\text{m}^{-1}$  and (b)  $\sigma_c = \kappa_c = 0.5 \text{ S}\cdot\text{m}^{-1}$ . The gray line (zero line) represents the case of  $\psi^* = 0$ , corresponding to case (iii). The region above the gray line stands for the condition of  $\psi^* > 0$ , corresponding to case (i). The region below the gray line stands for the condition of  $\psi^* < 0$ , corresponding to case (ii). The red line represents the  $\psi^*$  from 1 to 20C (red dots). The black solid line shows  $\psi^*$  from 0 to 1C as a reference since this current range does not match the Tafel approximation. The blue dot denotes the intersection between  $\psi^*$  and the gray line. (For interpretation of the references to colour in this figure legend, the reader is referred to the Web version of this article.)

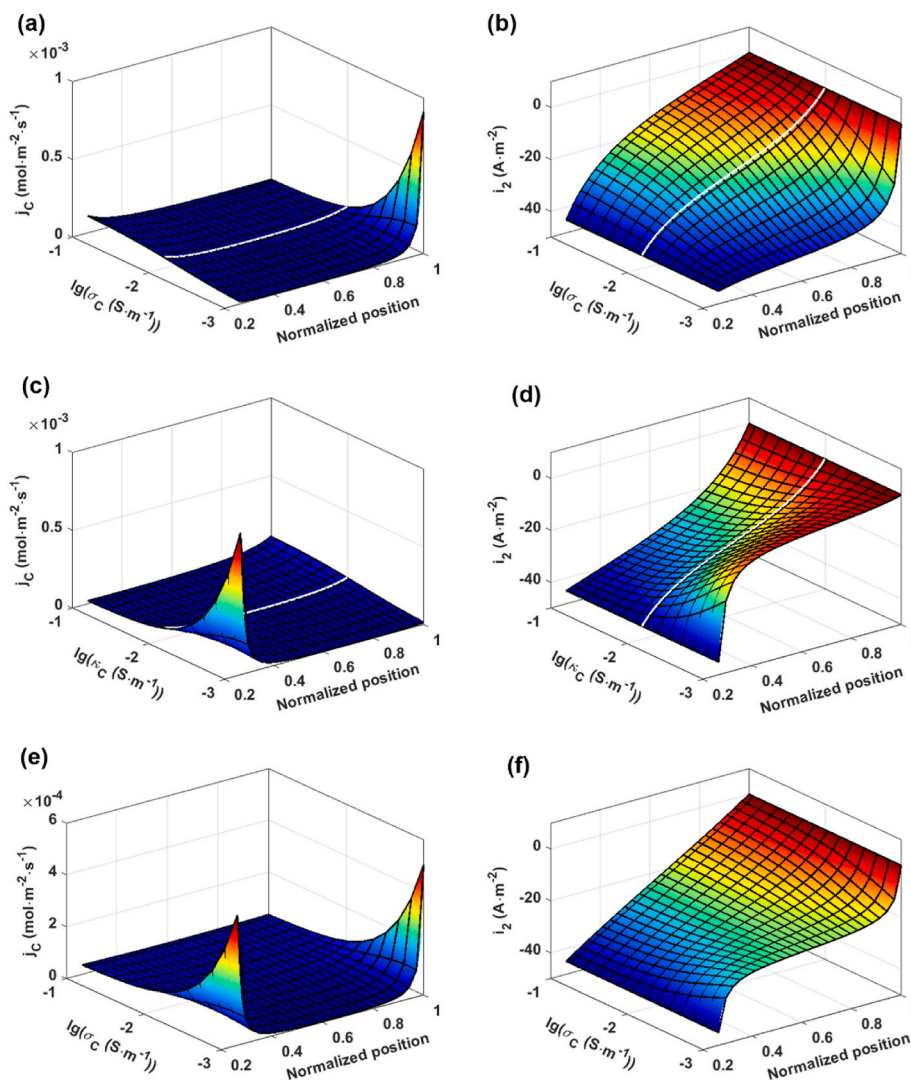


**Fig. 3.** The visualization of (a, c, and e) reaction-rate  $j_C$  and (b, d, and f) current-density  $i_2$  distributions inside the porous electrode as a function of effective electronic ( $\sigma_C$ ), ionic conductivities ( $\kappa_C$ ) and normalized position. In (a, b), the conductivity values are  $\kappa_C = 10^{-2} \text{ S m}^{-1}$  and  $\sigma_C = 10^{-3}$ – $10^{-1} \text{ S m}^{-1}$ . In (c, d), conductivities are with  $\sigma_C = 10^{-2} \text{ S m}^{-1}$  and  $\kappa_C = 10^{-3}$ – $10^{-1} \text{ S m}^{-1}$ . In (e, f), conductivities are  $\kappa_C = \sigma_C = 10^{-3}$ – $10^{-1} \text{ S m}^{-1}$ . The white lines in (a–d) indicate the case of  $\kappa_C = \sigma_C$ .

$\sigma_C$  keeps as a small value, such as  $10^{-3} \text{ S m}^{-1}$ ,  $j_C$  shows a dominant distribution near the CC interface ( $x = 1$ ). When  $\sigma_C$  increases, the dominance of  $j_C$  at the CC interface decreases and finally disappears. The current density  $i_2$  shows a corresponding change with the increasing values of  $\sigma_C$ . Small value of  $\sigma_C$  makes  $i_2$  a sharp change near the CC interface. Increasing  $\sigma_C$  releases this sharp change at the CC interface.

Fig. 3c–d shows the opposite value selection of  $\sigma_C$  and  $\kappa_C$  as those shown in Fig. 3a–b.  $\sigma_C$  is kept as a constant  $10^{-2} \text{ S m}^{-1}$ , while  $\kappa_C$  ranges from  $10^{-3}$  to  $10^{-1} \text{ S m}^{-1}$ . A small value of  $\kappa_C$  leads to a dominant distribution of  $j_C$  near the SC interface ( $x = 0.26$ ). Increasing  $\kappa_C$  will release the dominance of  $j_C$  near the SC interface. Similarly, the current density  $i_2$  also shows a sharp change near the SC interface with a small  $\kappa_C$ . Increasing  $\kappa_C$  also releases the sharp change at the SC interface.

Fig. 3e–f shows  $j_C$  and  $i_2$  for a special case  $\kappa_C = \sigma_C$ . Both  $\sigma_C$  and  $\kappa_C$  range from  $10^{-3}$  to  $10^{-1} \text{ S m}^{-1}$ . It can be seen that in this specific case, the reaction rate is symmetric with respect to the mid-point of the electrode thickness ( $x = (L + \delta)/2$ ). When both  $\kappa_C$  and  $\sigma_C$  are very small,  $j_C$  show dominating distribution at both the SC and CC interfaces. When both conductivities increase, the reaction rate starts to move toward the inside of the electrode. At the same time, the values of  $j_C$  at both interfaces decrease. When both  $\kappa_C$  and  $\sigma_C$  are large enough, for

example,  $0.1 \text{ S m}^{-1}$  or above,  $j_C$  approaches a uniform distribution.

The charge-transfer reactions inside the porous electrode involve electronic and ionic transport, which can be analytically expressed by  $\sigma_C$  and  $\kappa_C$ . A small value of  $\sigma_C$  makes the electronic transport across the porous electrode difficult and, consequently, leads to a dominant reaction near the current-collector interface. On the contrary, a small value of  $\kappa_C$  leads to a sluggish ionic transport resulting in a prominent reaction near the separator interface. When both of  $\sigma_C$  and  $\kappa_C$  are small values, the electronic and ionic transport are difficult to occur therefore causing a compromised reaction distribution near both the separator and current-collector interfaces. When both  $\sigma_C$  and  $\kappa_C$  are large enough, the electrons and ions are easy to transport. Therefore, a distribution close to uniform can be found.

According to the notations given in Fig. 3, four limiting types of  $j_C$  and  $i_2$  are summarized in Fig. 4. These four limiting types are similar to those observed in the linear approximation of the Butler-Volmer equation [8]. When both  $\kappa_C$  and  $\sigma_C$  are large enough, the reaction is evenly distributed, as shown by type (i). A small value of  $\sigma_C$  leads to a dominant reaction near the CC interface shown by type (ii), while a small value of  $\kappa_C$  makes the reaction dominant near the SC interface, shown by type (iii). When both the values of  $\kappa_C$  and  $\sigma_C$  are small, the reaction is



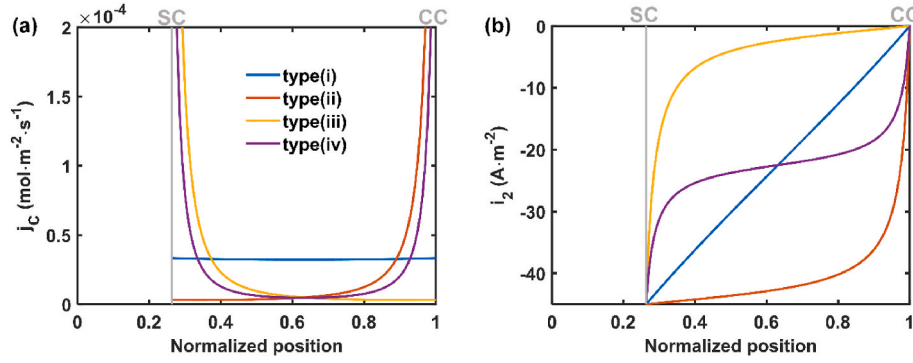


Fig. 4. Four limiting types of (a) the reaction-rate distribution  $j_c$  and (b) the current-density distribution  $i_2$  inside the porous electrode.

dominant at both the SC and CC interfaces (type (iv)). The  $i_2$  distribution also shows four different limiting types accordingly (Fig. 4b). The saturation phenomenon can still be observed. However, saturation values cannot be analytically expressed because of the influence of the current.

Two practical examples are presented to help illustrate the results. The ionic conductivity typical for Li-ion batteries ranges from 0 to 1 S m<sup>-1</sup>. The salt concentration in the electrolyte and the temperature also alter the ionic conductivity [12,13]. The electronic conductivity of LiFePO<sub>4</sub> (LFP) particles is as low as  $\sim 10^{-7}$  S m<sup>-1</sup> [14]. With the electrode porosity and Bruggeman coefficient considered, the effective electronic and ionic conductivities inside the porous electrode are even smaller. Conductive coatings are deposited on active particles, and conducting additives are added to improve the electronic conductivities and alleviate the nonuniformity of the reaction of the LFP electrode. For graphite electrodes, a relatively high effective electronic conductivity and a low effective ionic conductivity cause a dominant reaction near the separator/electrode interface.

Aside from  $\kappa_c$  and  $\sigma_c$ , the applied current  $I$  is another important factor influencing  $j_c$  and  $i_2$ , as shown by Eqs. (26) and (27) for case (i), Eqs. (34) and (35) for case (ii), and Eqs. (40) and (41) for case (iii). To make  $j_c$  and  $i_2$  comparable at different C-rates, the normalized reaction rate  $j_c/j_c^u$  and current density  $i_2/I$  are compared. Note that  $j_c^u$  represents the uniform reaction-rate distribution, which is defined by Eq. (42).  $j_c/j_c^u$  and  $i_2/I$  in case (i) can therefore be expressed by Eq. (44) and (45). For the other cases, similar expressions can be obtained.

$$j_c/j_c^u = -\frac{Ih^2A^2}{2(L-\delta)} \left[ 1 + \left( \tan \left[ \frac{Ih^2}{2}A(x-\delta) + \text{atan} \left( \frac{1-\gamma}{A} \right) \right] \right)^2 \right] \quad (44)$$

$$i_2/I = A \tan \left[ \frac{Ih^2}{2}A(x-\delta) + \text{atan} \left( \frac{1-\gamma}{A} \right) \right] + \gamma \quad (45)$$

Notably, both the ratios of  $j_c/j_c^u$  and  $i_2/I$  are a function of applied

current. Fig. 5 shows  $j_c/j_c^u$  and  $i_2/I$  at different C-rates with the condition of  $\kappa_c = \sigma_c = 10^{-1}$  S m<sup>-1</sup>. At 0.5 and 1 C-rate, the reaction rate is close to the uniform distribution. The current density is also linearly distributed. Increasing applied currents to 5 and 10C makes the  $j_c/j_c^u$  nonuniform, and the current densities become non-linearly distributed accordingly.

Besides  $\kappa_c$ ,  $\sigma_c$ , and  $I$ , other parameters of the porous electrode, such as specific area (a) and thickness of the porous electrode ( $L - \delta$ ), also matter in determining the reaction-rate and current-density distributions.

In practical applications achieving uniform reaction distribution is always beneficial for the energy/power output. Only in such a case the active materials can be fully utilized at particular (dis)charging conditions. Therefore, achieving uniform reaction distribution is essential for designing high-energy/power Li-ion batteries [15,16]. For a high-energy battery, using moderately high conductivities can be helpful to fully extract the energy since low C-rates are the most commonly used scenario. The design with high conductivities is also beneficial for high-power batteries because the intermediate and high C-rates are the target.

## 5. Conclusions

In the present paper, a rechargeable battery made of a single porous electrode and a flat metallic lithium counter-electrode is considered to investigate a particular case of reaction-rate and current-density distributions in the porous electrode. The explicit mathematical expressions for the reaction-rate distribution inside the porous electrode are obtained for a short moment after switching on the current. Two assumptions are used. Battery assumed to reside in equilibrium before the current is switched on. No concentration gradients or current flows exist before the moment of applying currents. Applying a Tafel approximation to the Butler-Volmer equation produces three different analytical solutions for the reaction-rate and current-density distributions. These three

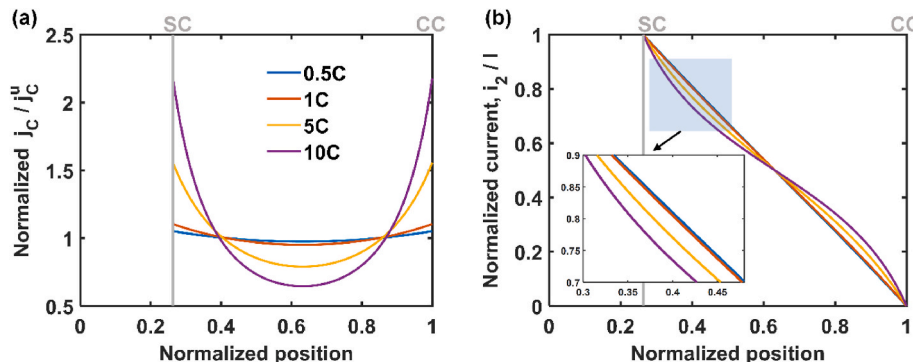


Fig. 5. Normalized (a) reaction-rate distribution  $j_c/j_c^u$  and (b) current-density distribution  $i_2/I$  at different C-rates with the condition  $\kappa_c = \sigma_c = 0.1$  S m<sup>-1</sup>.

solutions can be applied separately depending on the value of the CDC. The design parameters of the porous electrode and the applied current (density) determine the CDC value. In most of the scenarios, case (i) applies. The effective electronic and ionic conductivity values shift the reaction rate between the SC and CC interfaces, resulting in four limiting types. In addition, the applied current also influences the reaction-rate and current distributions. Large C-rates increase the nonuniformity of reaction-rate distribution and non-linearity of current distribution in porous electrodes.

#### CRediT authorship contribution statement

**Zhiqiang Chen:** Investigation, Software, Validation, Data curation, Writing – original draft, preparation. **Dmitri L. Danilov:** Conceptualization, Methodology, Software, Supervision, Writing – review & editing. **Rüdiger-A. Eichel:** Project administration. **Peter H.L. Notten:** Conceptualization, Supervision.

#### Declaration of competing interest

The authors declare that they have no known competing financial interests or personal relationships that could have appeared to influence the work reported in this paper.

#### Data availability

Data will be made available on request.

#### Acknowledgments

Dr. Z. Chen gratefully acknowledges the fellowship support of the China Scholarship Council. Dr. D.L. Danilov appreciates the support from the German Federal Ministry for Economic Affairs and Energy, within the project LImES, grant number 03ETE019E. The authors would

like to thank Dr. Luc H.J. Raijmakers from Fundamental Electrochemistry (IEK-9), Forschungszentrum Jülich, Germany, for his help in purchasing and communicating with EL-Cell GmbH.

#### References

- [1] Y. Ding, Z.P. Cano, A. Yu, J. Lu, Z. Chen, Automotive Li-ion batteries: current status and future perspectives, *Electrochem. Energy Rev.* 2 (2019) 1–28.
- [2] G. Assat, J.-M. Tarascon, Fundamental understanding and practical challenges of anionic redox activity in Li-ion batteries, *Nat. Energy* 3 (2018) 373–386.
- [3] A. Vu, Y. Qian, A. Stein, Porous electrode materials for lithium-ion batteries - how to prepare them and what makes them special, *Adv. Energy Mater.* 2 (2012) 1056–1085.
- [4] W.B. Hawley, J. Li, Electrode manufacturing for lithium-ion batteries—analysis of current and next generation processing, *J. Energy Storage* 25 (2019), 100862.
- [5] J. Newman, W. Tiedemann, Porous-electrode theory with battery applications, *AIChE J.* 21 (1975) 25–41.
- [6] J. Newman, C.W. Tobias, Theoretical analysis of current distribution in porous electrodes, *J. Electrochem. Soc.* 109 (1962) 1183–1191.
- [7] R. Darling, J. Newman, On the short-time behavior of porous intercalation electrodes, *J. Electrochem. Soc.* 144 (1997) 3057–3063.
- [8] Z. Chen, D.L. Danilov, R.-A. Eichel, P.H.L. Notten, On the reaction rate distribution in porous electrodes, *Electrochem. Commun.* 121 (2020), 106865.
- [9] Z. Chen, D.L. Danilov, R.-A. Eichel, P.H.L. Notten, Li+ Concentration Waves in a Liquid Electrolyte of Li-Ion Batteries with Porous Graphite-Based Electrodes, vol. 48, *Energy Storage Mater.*, 2022.
- [10] M. Doyle, T.F. Fuller, J. Newman, Modeling of galvanostatic charge and discharge of the lithium/polymer/insertion cell, *J. Electrochem. Soc.* 140 (1993) 1526–1533.
- [11] T.F. Fuller, M. Doyle, J. Newman, Simulation and optimization of the dual lithium ion insertion cell, *J. Electrochem. Soc.* 141 (1994) 1–10.
- [12] L.O. Valoen, J.N. Reimers, Transport properties of LiPF<sub>6</sub>-based Li-ion battery electrolytes, *J. Electrochem. Soc.* 152 (2005) A882–A891.
- [13] E. Prada, D. Di Domenico, Y. Creff, J. Bernard, V. Sauvant-Moynot, F. Huet, Simplified electrochemical and thermal model of LiFePO<sub>4</sub>-graphite Li-ion batteries for fast charge applications, *J. Electrochem. Soc.* 159 (2012) A1508–A1519.
- [14] C. Wang, J. Hong, Ionic/electronic conducting characteristics of LiFePO<sub>4</sub> cathode materials, *Electrochem. Solid State Lett.* 10 (2007) A65–A69.
- [15] F. Wu, M. Liu, Y. Li, X. Feng, K. Zhang, Y. Bai, X. Wang, C. Wu, High-mass-loading electrodes for advanced secondary batteries and supercapacitors, *Electrochem. Energy Rev.* 4 (2021) 382–446.
- [16] Y. Kuang, C. Chen, D. Kirsch, L. Hu, Thick electrode batteries: principles, opportunities, and challenges, *Adv. Energy Mater.* 9 (2019), 1901457.